Journal of Great Lakes Research 37 (2011) 707–716

Contents lists available at SciVerse ScienceDirect

Journal of Great Lakes Research

journal homepage: www.elsevier.com/locate/jglr

Evaporation from Lake Superior: 1. Physical controls and processes

Peter D. Blanken [a,*], Christopher Spence [b,1], Newell Hedstrom [b,2], John D. Lenters [c,3]

[a] Department of Geography and Program in Environmental Studies, University of Colorado, Boulder, CO 80309-0260, USA
[b] Environment Canada, Saskatoon, SK, Canada S7N 3H5
[c] School of Natural Resources, University of Nebraska-Lincoln, Lincoln, NE 68583-0987, USA

ARTICLE INFO

Article history:
Received 22 April 2011
Accepted 19 August 2011
Available online 2 October 2011

Communicated by Leon Boegman

Index words:
Energy balance
Evaporation
Great Lakes
Ice cover
Lake Superior
Water levels

ABSTRACT

The surface energy balance of Lake Superior was measured using the eddy covariance method at a remote, offshore site at 0.5-h intervals from June 2008 through November 2010. Pronounced seasonal patterns in the surface energy balance were observed, with a five-month delay between maximum summer net radiation and maximum winter latent and sensible heat fluxes. Late season (winter) evaporation and sensible heat losses from the lake typically occurred in two- to three-day-long events, and were associated with significant release of stored heat from the lake. The majority of the evaporative heat loss (70–88%) and sensible heat loss (97–99%) occurred between October and March, with 464 mm (2008–2009) and 645 mm (2009–2010) of evaporative water loss occurring over the water year starting October 1. Evaporation was proportional to the horizontal wind speed, inversely proportional to the ambient vapor pressure, and was well described by the ratio of wind speed to vapor pressure. This ratio remained relatively constant between the two water years, so the differences in evaporative water loss between years were largely associated with differences in lake surface conditions (e.g. water temperature, ice cover, and ice duration). Since late-season water temperature decline is driven by evaporative and sensible heat loss, the potential for a negative feedback mechanism between evaporation and ice cover is discussed.

Introduction

Lake Superior has a surface area of 82,100 km^2, making it the largest freshwater lake in the world, by surface area (Kalff, 2002). Together with the other Great Lakes, the socioeconomic importance of this resource is immense for both the United States and Canada, directly influencing sectors including power production, navigation, industry, commercial operations, agriculture, and recreation (Hartmann, 1990). The economic impact of the Great Lakes is large; for example, spending on recreational boating in 2003 alone was $9.4 billion, and created 60,000 jobs (US Army Corps of Engineers, 2008). The importance of the Great Lakes to the regional meteorology and climate is significant for both countries, since changes in meteorological conditions and water quality often directly impact the economy of the region. Examples include changes in ice cover (Assel et al., 2003) which, in-turn, are linked to lake-enhanced snow events (Cordeira and Laird, 2008; Ellis and Johnson, 2004) affecting transportation; and decreases in water level through recent increases in evaporation (Hanrahan et al., 2010; Sellinger et al., 2008) affecting navigation and shore-line erosion.

Despite the significance of the Great Lakes, the boundary conditions at the air–lake interface that drive the surface meteorology and limnology through the surface energy balance are seldom directly measured, especially for large lakes such as Lake Superior. This is not because the surface energy balance is not recognized as being important, but rather is due to the limited availability of required measurements on the lake itself, and most hydroclimate models still require forcing data from direct measurements (e.g. Huang et al., 2011). As we show here, the magnitude and dynamics of the heat exchange between the air–lake interface are greatest during the winter when buoy-based meteorological measurements are not available. Therefore, much of the past research on the surface energy balance of Lake Superior and other large lakes has been based on empirical models (e.g. Derecki, 1981), buoy-based measurements during the open-water season (e.g. Laird and Kristovich, 2002), or more complex hydrodynamic models (e.g. Beletsky et al., 1999), aided by remotely-sensed data when available (e.g. Lofgren and Zhu, 2000; Nghiem and Leshkevich, 2007).

What is lacking from most previous studies is a direct measurement of the evaporative and sensible heat losses (i.e., more than just bulk aerodynamic relationships), especially during the winter months when these losses are at maximum. The value of such measurements is that they provide an understanding of the temporal patterns of the surface energy balance, and the physical controls of the processes

* Corresponding author. Tel.: +1 303 492 8310.
E-mail addresses: blanken@colorado.edu (P.D. Blanken), Chris.Spence@ec.gc.ca (C. Spence), Newell.Hedstrom@ec.gc.ca (N. Hedstrom), jlenters2@unl.edu (J.D. Lenters).
[1] Tel.: +1 306 975 6907.
[2] Tel.: +1 306 975 6049.
[3] Tel.: +1 402 304 0166.

0380-1330/$ – see front matter
doi:10.1016/j.jglr.2011.08.009

involved. This understanding can then be used to verify, calibrate, and improve the predictive models. It is the purpose of this paper, therefore, to describe the annual patterns of direct measurements of the surface energy balance of Lake Superior, and to understand the first-order controls on the evaporative water loss. Although we describe direct measurements based on the eddy covariance method from a remote site 39-km offshore, our measurements represent an upwind distance of roughly 6 km. The controls on evaporation that we discuss may vary significantly on the spatial scale of this immense lake, therefore any efforts to model the evaporative process over a broad area requires knowledge of the spatial patterns in the atmospheric driving variables and lake temperature. The companion paper by Spence et al. (in press) deals with this aspect of the study.

There are several studies reporting that Lake Superior is responding to climate change. Schertzer and Rao (2009) provide a summary of the past and present state of the Lake; their review can be used as a baseline for climate change modeling or historical trend-analysis studies. Examples of recent studies describing the contemporary changing conditions include Bennington et al. (2010), who used a Reynolds-averaged hydrodynamic model to simulate and analyze circulation in Lake Superior from 1979 to 2006. They simulated increasing lake surface and above-lake air temperatures at a rate of 0.34 and 0.8 °C per decade, respectively, increasing wind speed (0.18 m s^{-1} per decade), and a long-term decline in January–April ice cover (−866 km^2 per year). Austin and Colman (2007), on the other hand, found even larger increases in buoy-measured lake temperature over a similar time period, and at a rate that was higher than that of the above-lake air temperatures, rather than lower. Trend-analysis studies show that snowfall has increased dramatically in areas that are subject to lake-effect snowfall (Ellis and Johnson, 2004), although it has been noted that such trends should be treated with caution (Kunkel et al., 2007). Water levels have been decreasing at a rate of approximately 1 cm per year from 1970 to 2005 (Moitee and McBean, 2009), while at the same time experiencing shifts in the seasonal cycle (Argyilan and Forman, 2003; Lenters, 2001, 2004; Quinn, 2002). Given these and other changes, the purpose of this paper is to describe the annual surface energy balance of Lake Superior based on direct measurements, and to discuss how the physical processes regulating the surface energy balance may be affected by climate change.

Materials and methods

Making year-long, over-water measurements on Lake Superior, the deepest (mean depth 148 m; maximum depth 406 m) and largest (surface area 82,100 km^2; volume 12,100 km^3) of the Great Lakes, is exceptionally difficult for logistical, cost, and safety reasons. Stannard Rock Light (47.183506, −87.22511), however, a historic lighthouse located on a shoal 39 km from the nearest shore (the Keweenaw Peninsula) provided an ideal location for this project. The now-automated lighthouse, completed in 1882, offers a stable, year-round platform for the meteorological and eddy covariance instruments, as well as good conditions for surface flux measurements, given its location (far from shore), its height (32.4 m above the mean water level), and the absence of any underlying land surface (i.e. island) to influence measurements. Although shallow water (~5 m deep) surround the immediate area, water depths within the source area for the flux measurements (~6 km upwind during the active evaporation season; see below) range from 150 to 300 m. The eddy covariance and supporting meteorological measurements reported here were made between June 12, 2008 and November 4, 2010.

From a mast fastened to the top of the lighthouse structure 32.4 m above the water surface, the turbulent fluxes of sensible (H) and latent (λE) heat were calculated from 10-Hz measurements of the vertical wind speed (w) and the water vapor density (q). Wind speed was measured using a 3-D sonic anemometer (model CSAT-3, Campbell Scientific, Logan, UT), while water vapor density was measured using an open-path gas analyzer (model LI-7500, LI-COR Biosciences, Lincoln, NE) located 15 cm away and at the same height as the sonic anemometer. The statistics (means and covariances) of the high-frequency sampled data were collected at 30-min intervals using a datalogger (model CR3000, Campbell Scientific, Logan, UT), with DC power provided by eight 12-V deep-cycle marine batteries charged by six 80-W solar panels. The datalogger and batteries were located in a dry location inside the lighthouse. Post-processing of these data, including quality control, is described below.

On the same mast, slow 5-s samples of ancillary meteorological variables were also measured, with 30-min statistics collected on the same datalogger as the high-frequency data. Air temperature (T_a; °C) and humidity (vapor pressure, e_a; kPa) were measured with a shielded probe (model HMP45C, Vaisala, Helsinki), and barometric pressure (P; kPa) was measured with a pressure transducer located inside the electronics box of the LI-7500. The horizontal wind speed (U; m s^{-1}) and direction were measured with a wind vane (model 05103, RM Young, Traverse City, MI), in addition to horizontal wind speed and direction calculated from the sonic anemometer data. Water surface temperature (T_o) was measured with an infrared thermometer (model IRR-P, Apogee, Logan, UT). At times (29% of all the 0.5-h measurements), the measured T_o was unreliable likely due to condensation or frost formation inside the instrument cavity. Water surface temperature was estimated during such times by solving the stability-corrected flux-gradient equation (Businger et al., 1971) using the measured sensible heat flux and two levels; the water surface and instrument heights. The incident short-wave ($S\downarrow$) and long-wave radiation ($L\downarrow$) were measured with radiometers (models SP Lite and CGR-4, respectively, Kipp and Zonen, Delft).

Lake-wide daily ice cover was estimated from the NOAA-GLERL Great Lakes Ice Atlas, which provides the percentage of a nominal 2.55 km × 2.55 km grid covered by ice based on a blend of observations from several data sources including ships, aircraft, and satellites (Assel, 2005). The daily ice cover percentages were also estimated within the ~6-km turbulent flux footprint of the eddy covariance instruments (described in the Theory/calculation section), using georeferenced ice charts provided by the Canadian Ice Service.

Theory/calculation

The turbulent fluxes of latent and sensible heat (W m^{-2}) were calculated from the covariance of the high-frequency measurements of the vertical wind speed (m s^{-1}) with water vapor density (g m^{-3}) or virtual air temperature (T; °C), respectively:

$$\lambda E = \overline{\lambda w' q'} \quad (1)$$

$$H = \overline{\rho c w' T'} \quad (2)$$

where λ is the air temperature-dependent latent heat of vaporization (J g^1), ρ is the dry air density (g m^{-3}), c is the pressure-dependent specific heat of dry air (J g^{-1} °C^{-1}), and primes denote deviations from the 30-min non-overlapping, non-detrended means (overbars). Positive values indicate turbulent fluxes directed away from the surface; negative towards. The 30-min averaging period was chosen since we found that period gave good energy balance closure at an offshore site (~12 km) over the similarly large Great Slave Lake (Blanken et al., 2000), where intermittent high-frequency turbulent events played a significant role in evaporation (Blanken et al., 2003). Since our site was also far from shore where there was no sharp contrast in thermal and roughness characteristics, we did not expect contributions to the turbulent fluxes created by low-frequency turbulence that would require a longer averaging period (e.g. 1 h; Nordbo et al., 2011). The covariance between w and q or T were first mathematically rotated so that the 30-min mean w and v (crosswind component) were zero using the procedure described in Baldocchi et al. (1988). Then λE was

adjusted to account for the effects of air density fluctuations (Webb et al., 1980). Lastly, a transfer function (Horst, 1997) based on the scalar flux time constant (Massman, 2000) was applied to account for flux attenuation due to sensor path length and separation between the CSAT-3 and LI-7500.

Net radiation, given by

$$R_n = S\downarrow(1-\alpha) + L\downarrow - L\uparrow \quad (3)$$

was calculated using the measured $S\downarrow$ and $L\downarrow$, with shortwave albedo (α) set to 0.07 during ice-free conditions based on direct measurements made over nearby Lake Huron (α of 0.80, weighted by ice fraction, was used for the ice-covered area within 6 km of the site), and $L\uparrow$ was calculated using the Stefan–Boltzmann Law ($L\uparrow = \varepsilon\sigma T_0^4$ where σ is the Stefan–Boltzmann constant) using an emissivity (ε) of 0.98 and the water surface temperature (T_o in Kelvin). The heat storage term (J_s; W m^{-2}) was estimated as a residual of the energy balance:

$$J_s = R_n - \lambda E - H. \quad (4)$$

Although calculating J_s as a residual does incorporate all of the errors in the other energy balance terms, it is likely within 10–20% of the actual heat storage term based on energy balance closure measurements reported from others that use the eddy covariance method (Tanny et al., 2007). Our values of J_s also compare very well with those calculated by Schertzer (1978) using measured water temperature profiles, giving us additional confidence in our measured energy balance terms.

The distance upwind that contributed to λE and H (otherwise known as the turbulent flux footprint) was estimated using the solutions of the diffusion equations given by Schuepp et al. (1990). Corrections to their equations for atmospheric stability were made based on the median value of the dimensionless stability parameter $\zeta = z/L$, where z is the measurement height (32.4 m) and L is the Obukhov stability length. Based on these calculations, during unstable atmospheric conditions (when the majority of λE and H occurred), the upwind distance that the flux measurements were most sensitive to was found to be 674 m, and 80% of the total flux was obtained over an upwind distance of 6 km. Relative to the immense size of the lake, this is a relatively small distance to sample. The companion paper by Spence et al. (in press), however, explicitly addresses the spatial variation in λE across the lake using a combination of modeling, remote sensing, and GIS techniques.

Results

The energy balance and flux measurements obtained during the 2.5-year observation period are a unique dataset, as the only other continuous, over-lake observations (from a few island-based sites) do not generally contain such detailed information on radiative, sensible, and latent heat fluxes. As noted earlier, buoy-based measurements are not available during the meteorologically active late fall/winter periods, since they are only deployed from April through November. The general conditions observed from 2008 to 2010 were typical of those over (or near) a large continental North American lake (Fig. 1; Table 1). Summers were relatively warm and humid, with light-to-moderate winds. Atmospheric pressure, although variable throughout the year, displayed the least variance during the summer compared to the winter months (0.5-h mean std dev 0.51 kPa JJA, compared to 0.92 kPa DJF). In contrast, the atmosphere during the fall and winter periods was cold, dry, and windy. During the October 1 through March 31 winter evaporation season, the mean T_a and e_a were −1.72 °C and 0.47 kPa in 2009–2010, compared to 0.432 °C and 0.52 kPa in 2008–2009, respectively.

The surface energy balance components also displayed a strong seasonal pattern (Fig. 2; Table 1), as the surface energy balance was

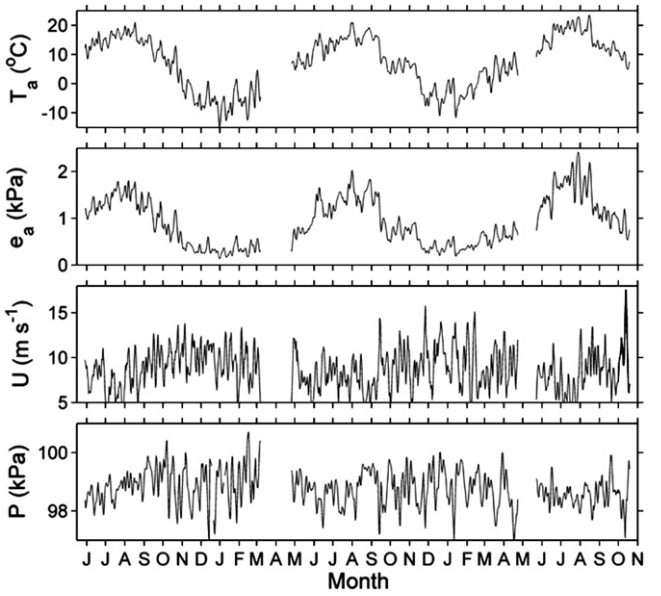

Fig. 1. Three-day running means of half-hour measurements of basic meteorological conditions from June 12, 2008 through November 4, 2010; air temperature (T_a), vapor pressure (e_a), horizontal wind speed (U), barometric pressure (P). Mid-months are labeled.

largely driven by over-lake meteorological and lake surface conditions (e.g. surface water temperature and ice cover). Net radiation peaked near the summer solstice, and reached a winter-time minimum near the winter solstice. In contrast, λE and H were near zero when R_n was at its seasonal maximum (Fig. 2); λE and H reached their seasonal maximums in the winter period (DJF), when R_n was near zero. Both λE and H had roughly three-day-long "events" (see Fig. 7) similar to that found over Great Slave Lake (Blanken et al., 2000; 2003), with the evaporation season lasting from late August through March. Most of the net radiation during the February through October period (when the 24-h mean $R_n > 0$ W m^{-2}) was partitioned not as λE or H, but as the storage term (J_s), representing the energy used (released) to heat (cool) the lake water. During the summer months when R_n was largest, nearly all of that energy was used to warm the water, since turbulent fluxes were essentially negligible (and even negative, in some instances). During the winter months, the energy to fuel the large λE and H events was drawn from the large store of internal energy contained within the warm lake water (relative to air), since R_n was essentially zero at that time.

With the water surface warmer than the air during the winter months, the atmosphere was thermally unstable ($\zeta < 0$) with turbulence mixing driven by convection as indicated by the positive and large H. During the water year (beginning October 1), the atmosphere was unstable most of the time (61 and 64% of the 0.5-h measurements, 2008–2009 and 2009–2010 water years, respectively), with the majority of the total water years' evaporative water loss occurring during these unstable periods (92%; 425 mm, and 89%; 575 mm, 2008–2009 and 2009–2010 water years, respectively). In general, evaporative heat losses occurred only when the atmosphere was unstable, and the atmosphere become progressively more unstable and evaporation increased as the season progressed through the winter months (Fig. 3).

The delay, or temporal lag, between energy inputs into the lake and energy outputs from the lake, is explicitly shown in Fig. 4. The 24-h mean detrended time series of R_n and H has the highest correlation coefficient at a lag of 147 days, while the lag is 154 days between R_n and λE. Thus, there was approximately a five-month delay between the time of maximum energy input into the lake and the time of maximum energy output from the lake. This is primarily due to the high specific heat of water and the large mean depth of Lake Superior.

Table 1
Summary of the surface energy balance and meteorological conditions based on 0.5-h measurements from October 1, 2008 through September 30, 2009 (Year 1), and October 1, 2009 through September 30, 2010 (Year 2). All means were significantly different at a 5% significance level (two-tailed *t*-test; unequal variance).

	Mean		Median		Standard deviation		Maximum		Minimum	
	Year 1	Year 2	Year 1	Year 2	Year 1	Year 2	Year 1	Year 2	Year 1	Year 2
R_n (W m^{-2})	96.4	84.9	4.1	−0.8	200.5	196.2	843.2	798.5	−99.1	−115.8
λE (W m^{-2}) and total (mm)	49.4 (464)	57.1 (645)	27.0	37.2	102.9	120.8	n/a	n/a	n/a	n/a
H (W m^{-2})	40.0	30.8	8.62	9.34	89.0	80.0	n/a	n/a	n/a	n/a
J_s (W m^{-2})	14.8	−1.8	−33.3	−50.1	288.9	277.2	n/a	n/a	n/a	n/a
T_a (°C)	5.07	6.59	6.53	6.20	9.84	8.91	26.93	28.87	−16.31	−15.76
e_a (kPa)	0.82	0.89	0.72	0.69	0.52	0.57	2.45	2.68	0.11	0.11
P (kPa)	98.8	98.7	98.9	98.7	0.85	0.77	101.1	100.6	95.7	95.3
U (m s^{-1})	8.91	8.78	8.73	8.56	4.09	4.08	42.7	34.1	0.41	0.23
Ice coverage (%)							90	31		
Lake-wide ice on dates	Dec 9, 2008	Dec 8, 2009								
Stannard Rock ice on dates	Jan 23, 2009	n/a								
Lake-wide ice off dates	May 7, 2009	Apr 14, 2010								

The effect of the delay between energy input and output is apparent in both the cumulative evaporative water loss (E; mm equivalent over the water year starting October 1) and sensible heat (for comparative purposes also expressed as a mm equivalent) (Fig. 5). For both the 2008–2009 and 2009–2010 water years, the majority of the evaporation and sensible heat loss from the lake occurred between October and March; 88% (2008–2009) and 70% (2009–2010) of the water years' total losses for E (464 and 645 mm, 2008–2009 and 2009–2010 totals, respectively); 99% (2008–2009) and 97% (2009–2010) of the water years' total losses for H (374 and 345 mm, 2008–2009 and 2009–2010 totals, respectively). These water-year totals for E are similar to the average 500 mm per year reported by a variety of indirect methods (Schertzer and Rao, 2009). At the end of the maximum heat loss period in mid-March, the evaporative water losses were 406 mm (March 15, 2009) and 448 mm (March 15, 2010). Sensible heat losses (mm equivalent) also differed by about 10% between the two years, but unlike the evaporative losses, were higher in 2009 than in 2010 (372 mm in 2009, and 335 mm in 2010).

Fig. 6 shows that both the lake-wide and near-site ice coverage during the 2008–2009 winter were much higher (maximum 90% and 95%, lake-wide and near-site, respectively) than the long-term (1973–2010) climatological average (maximum 51%) throughout much of the winter. Compared to the lake-wide averages, ice coverage was more variable, with later formation and earlier break-up dates. In contrast, the following winter (2009–2010) had a very low ice coverage (maximum 31%), and no ice was detected near the lighthouse measurement site. Thus, of the two October–March evaporation seasons, the one with the lower ice coverage had a higher total evaporation (but lower percentage of the water-year total), and a smaller loss of sensible heat.

A closer examination of Fig. 5 shows that the 2008–2009 water year actually had higher rates of sensible and evaporative heat flux up until mid-to-late December, at which point the cumulative fluxes were roughly equal between the 2 years. This greater loss of heat in the autumn of 2008 (as compared to 2009) likely contributed to the more extensive ice cover that formed later that winter. By early January, however, the cumulative evaporation for 2009–2010 began to overtake that of 2008–2009 (Fig. 5), likely as a result of the less extensive ice cover, thereby leading to the higher overall water loss by mid March. In contrast to evaporation, the relative trends in cumulative sensible heat flux for the 2 years did not reverse in late December. Rather, they remained similar through the month of January and then diverged in early February, with the sensible heat fluxes for 2008–2009 once again exceeding those for 2009–2010. Although 2009–2010 had less

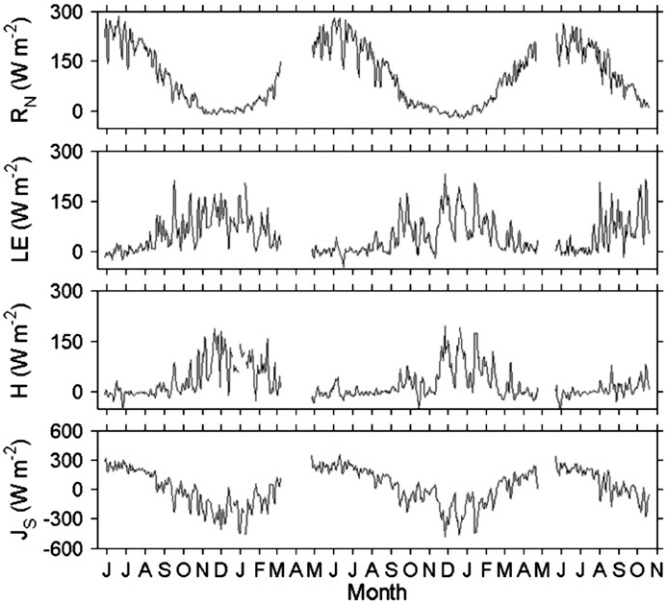

Fig. 2. Three-day running means of half-hour measurements of the surface energy balance from June 12, 2008 through November 4, 2010; net radiation (R_N), latent heat flux (λE), sensible heat flux (H), energy storage estimated as the residual of the energy balance (J_S). Mid-months are labeled.

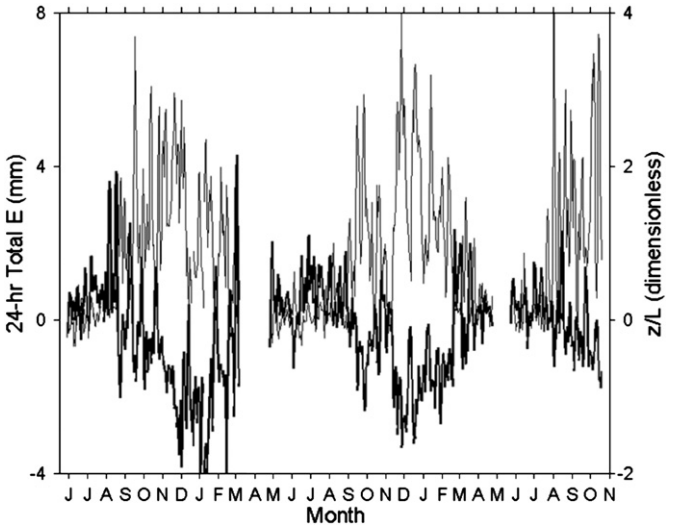

Fig. 3. Three-day running means of the 24-h total evaporation (thin lines) and the Obukhov stability parameter $\zeta = z/L$ (thick lines; positive = stable; negative = unstable) from June 12, 2008 through November 4, 2010. Mid-months are labeled.

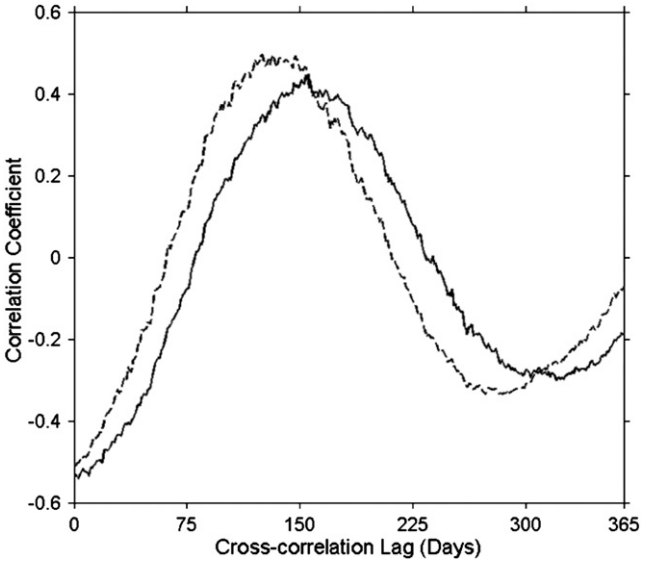

Fig. 4. Cross-correlations between the 24-h mean linear detrended net radiation and latent heat flux (λ*E*; solid line); and the 24-h mean linear detrended net radiation and sensible heat flux (*H*; dashed line). Maximum correlation coefficients were obtained with a lag of 147 and 154 days for *H* and λ*E*, respectively.

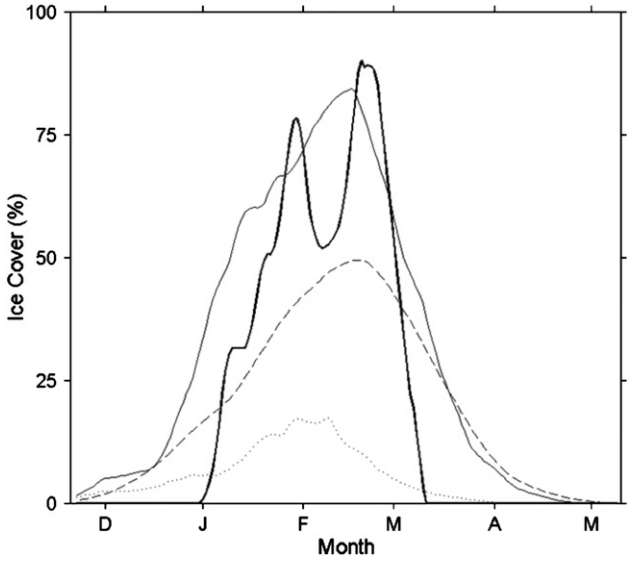

Fig. 6. 15-day running means of the percentage of the lake-wide ice cover for 2008–2009 (thin solid line), 2009–2010 (dotted line), and the 1973–2010 climatological mean (dashed line). Ice cover within the turbulent flux footprint radius (6 km) for 2008–2009 (thick solid line). No ice was present within the 6-km radius during 2009–2010. Mid-months are labeled.

ice cover than 2008–2009, the considerably higher air temperatures during the late winter and early spring of 2010 (in association with a strong El Niño event) likely led to the lower rates of sensible heat loss (and thereby contributing to the reduced rate of ice formation). Thus, it is important to consider the seasonal timing and potential feedbacks between ice cover and surface heat fluxes when examining interannual variations (represented, in this case, by 2 years with significantly different amounts of ice cover).

Additional insight into the physical processes behind seasonal patterns of λ*E* and *H* can be obtained by looking at patterns in the temporal behavior of the 0.5-h mean time series. Fig. 7 shows the correlation coefficient of the individual 0.5-h mean λ*E* and *H* using the linearly detrended 0.5-h time series from June 12, 2008 through November 4, 2010, as the time series were shifted by various temporal lags. The autocorrelation functions stop decreasing at a time lag of approximately 2.5 and 3.0 days, for *H* and λ*E*, respectively. This implies that the average length of sensible and latent heat loss events were 2.5 and 3.0 days, respectively, (see Fig. 8) similar to the length of evaporation events reported by Blanken et al. (2008) from Great Slave Lake. Blanken et al. (2000) showed that the dominant meteorological variables driving λ*E* from Great Slave Lake, (also a large lake, with roughly one-third the surface area and mean depth of Lake Superior), were the horizontal wind speed and vapor pressure gradient. Fig. 8 shows three examples of the two- to three-day long evaporation events during the early (August 24–27, 2010), mid (October 9–12, 2009), and late (December 12–17, 2009) evaporation season, together with *U* and e_a, all measured at $z = 32.4$ m above the water surface. Note that as the evaporation season progressed, e_a decreased from relatively large values in August (humid) to low values in December (dry). The vapor pressure gradient between the water surface and air requires a

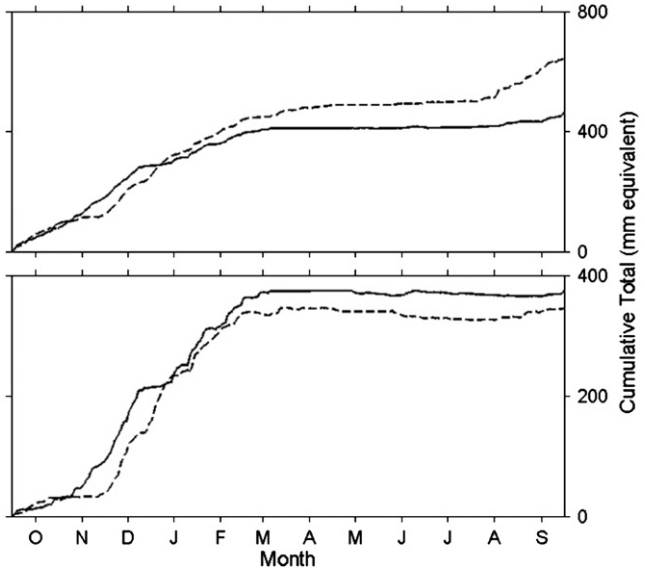

Fig. 5. Cumulative 0.5-h latent heat flux (top) and sensible heat flux (bottom) expressed as equivalent mm of water for the period October 1st through September 30th of 2008–2009 (solid line) and 2009–2010 (dashed line). Mid-months are labeled.

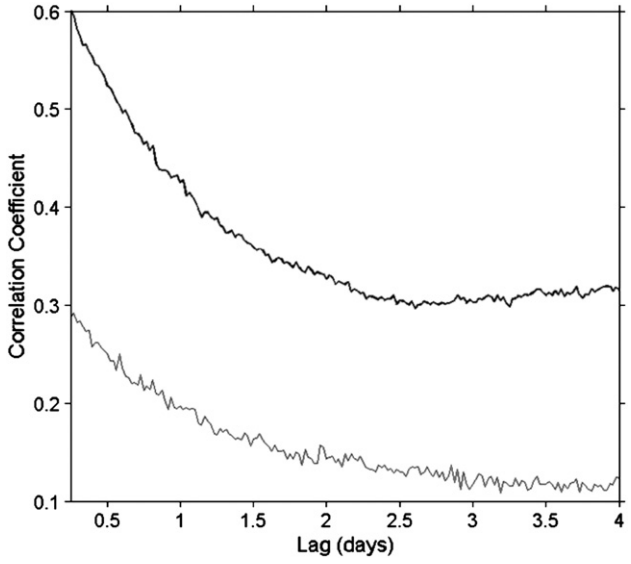

Fig. 7. Correlation coefficient (*r*) for the linear detrended lagged autocorrelation sequence for the sensible heat flux (thick line) and the latent heat flux (thin line) for all of the 0.5-h measurements taken over from June 12, 2008 through November 4, 2010. For clarity, plot starts at a lag of 0.25 days following the sharp decrease from $r = 1$ at lag = 0 days.

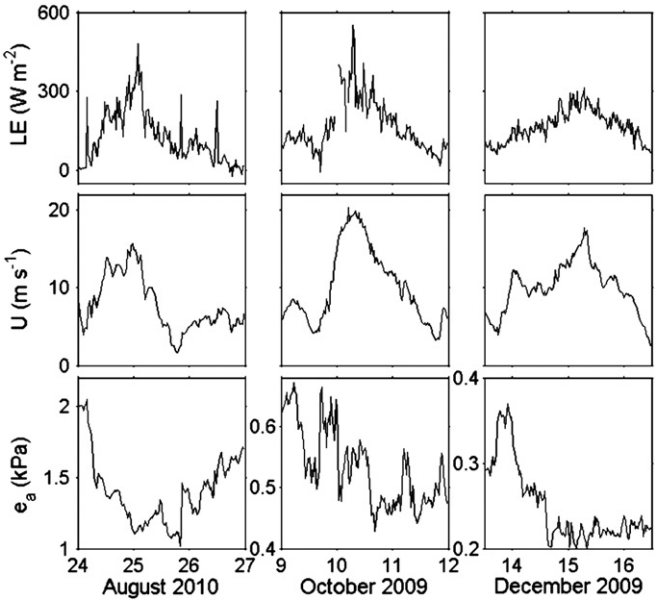

Fig. 8. Three examples of typical three-day evaporation events along a gradient of vapor pressures from high (12:00 pm August 24–12:00 pm August 27, 2010 EDT), to medium (12:00 pm October 9–12:00 pm October 12, 2009 EDT), to low (12:00 am December 14–12:00 am December 17, 2009 EDT). Half-hour means of the latent heat flux (λE), horizontal wind speed (U), and vapor pressure (e_a) measured at 32.4-m above the mean water surface, are shown. The atmosphere was became progressively thermally unstable as the season progressed, with median $\zeta = z/L$ values of −0.25 (August 2010), −1.02 (October 2009), −1.30 (December 2009).

measurement of the saturation vapor pressure of water, and therefore water surface temperature. This is preferably measured with an infrared thermometer so that the actual "skin" temperature of the water is measured. As described in the Materials and Methods section, due to condensation or frost inside the infrared thermometer, however, we found the water surface temperature measurements at Stannard Rock to be unreliable at times. Therefore, we based much of the analysis on only the ambient atmospheric vapor pressure, which is also more widely available and hence practical for applications at other lakes and times. In each example, λE increased from near-zero as U increased and e_a decreased, followed by a steady decrease in λE as U decreased and e_a increased (or remained unchanged).

Overall, λE was proportional to U, inversely proportional to e_a, and was described well by the ratio U/e_a (Fig. 9) during each of the examples shown in Fig. 8. As time progressed from August to December, U tended to increase and e_a tended to decrease (Fig. 1), so the relationship between λE and U/e_a, although linear and well-defined during individual events, varied through the year. This was largely due to the fact that periods of high e_a (and low U/e_a, such as in August) were also associated with higher water temperatures and, therefore, larger lake-air vapor pressure gradients and evaporation rates than would be expected based on e_a alone. The relationship between λE and e_a alone (Fig. 9, middle panel) was not well defined, especially when e_a was small. Small vapor pressures occurred predominantly during the winter when U was large (Fig. 1), and λE was more sensitive to U during these periods. The linear regression slopes and intercepts were similar, however, with a minimum correlation coefficient of 0.83 (Table 2; Fig. 10), when the 0.5-h mean λE and U/e_a were standardized by their respective maximum values. The relationship between the 0.5-h mean λE and U/e_a using all of the data for each of the water years (Fig. 11) showed a pattern similar to that shown in Figs. 9 and 10. For both years, the increase of λE was linear as a function of U/e_a; the slope, intercept, and correlation coefficients based on robust linear regressions of the 0.5-h data were 2.51 W m^{-2} m^{-1} s kPa, −1.27 W m^{-2}, and 0.55, for 2008–2009, and 3.31 W m^{-2} m^{-1} s kPa, −2.25 W m^{-2}, and 0.52, for 2009–2010. As shown by the frequency distributions in Fig. 11, there were few occurrences of large values of U/e_a, indicating that the highest evaporation rates tended to occur during fewer events.

To provide an estimate of the predictive ability of the functional relationship shown in Fig. 11, λE was calculated and compared to the measured λE for several days where both short-term (one day) and long-term (three-day) events occurred (Fig. 12). For comparison, two other relationships were used to calculate λE; one based solely on U, and the other based on $\lambda E/U$ being assumed proportional to $-e_a$. Both short- and long-term λE events were underestimated when only U was used as a predictor. Improvements were made when the $\lambda E/U$ versus e_a relationship was used, however, the long-duration λE event (January 1st through 8th) was not well captured. Of these three methods, the U/e_a version tracked the measured λE best, with a slope closest to unity, lowest y-intercept, and the highest r^2. This method, however, also had the highest RMSE (Table 3).

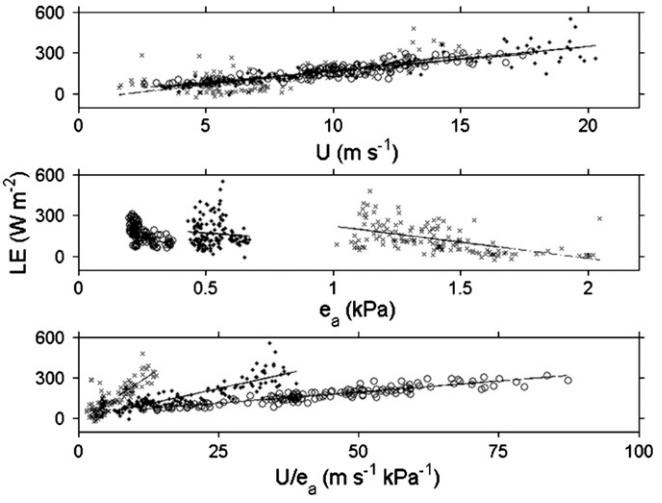

Fig. 9. Scatter plot (points) with linear regressions (lines) showing the relationship between the 0.5-h latent heat flux (λE) and the 32.4-m horizontal wind speed (U), vapor pressure (e_a) and ratio U/e_a. Shown are three example evaporation events (see Fig. 8) that occurred during October 9–12, 2009 (solid circles; solid lines), December 14–17, 2009 (open circles; dashed lines), and August 24–27, 2010 (crosses; dotted lines).

Discussion

The surface energy balance of a deep body of fresh water is unique when compared to smaller lakes and land surfaces. Whereas shallow lakes and land surfaces are tightly coupled to the diurnal cycle of net radiation, Lake Superior's large heat storage resulted in a five-month delay between maximum summer net radiation energy inputs and maximum release of that energy in winter in the form of latent (evaporative) and sensible heat fluxes. While the energy for the latent heat of vaporization was drawn from the thermal energy stored within the lake (negative J_s), the magnitude of the two- to three-day-long evaporation events was well represented by the ratio of U/e_a, with U increasing and e_a decreasing on time scales of 2 to 3 days. Although we did not perform a formal analysis here, this time scale likely represents the scale of the passage of synoptic-scale cold fronts, similar to that reported at more southern water locations (Liu et al., 2011).

During the summer ice-free season, Lake Superior has a low albedo, predominately clear skies, and low surface temperatures. Therefore, R_n is dominated by the incident solar radiation which in turn varies diurnally and seasonally through sun angle and day length. Maximum incident solar radiation occurs at the summer solstice, hence R_n generally reaches its maximum at this time as well (with minimum R_n occurring around the winter solstice). Near the summer solstice, however, the turbulent fluxes of sensible and latent heat are near zero since the lake's

Table 2
Statistics for linear regressions of the relationship between 0.5-h measured λE and U/e_a standardized by their respective maximum values as shown in Fig. 10.

Event dates	Maximum values			Linear regressions			
	λE (W m^{-2})	U (m s^{-1})	e_a (kPa)	Slope	Intercept	n (hrs)	r
Early season — August 24–27, 2010	480	15.7	2.05	0.795	−0.0664	71.5	0.83
Mid season — October 9–12, 2009	552	20.3	0.672	0.638	−0.014	69.5	0.87
Late season — December 14–17, 2009	313	17.8	0.369	0.914	0.0937	71.5	0.92

surface water is relatively cold, the atmosphere is relatively humid, and the winds are relatively calm (compared to winter-time conditions). Therefore, nearly all of the net radiation in spring and early summer is used to increase the water's temperature (i.e. the heat storage term), with a slow and minimal increase in the water temperature up to 4 °C, due to the water's high specific heat and deep, well-mixed water column. Beyond 4 °C, the lake becomes thermally stratified, and the upper mixed layer warms more rapidly. Not until late summer do the water surface temperatures become large enough to support significant latent and sensible heat flux.

Beginning roughly in late August and lasting through March, synoptic-scale frontal passages of cold air become more frequent as the seasons change. Variability in atmospheric pressure begins to increase, and as shown here, evaporative and sensible heat losses from the lake increase in proportion to the increase in horizontal wind speed, decrease in atmospheric vapor pressure, and increases in the lake/air temperature and vapor pressure gradients. The time scale for the passage of these cold fronts across the lake is 2 to 3 days, corresponding to the time scale for the evaporation events. The majority of the evaporative water and convective heat losses occur during this period (between October and March), with the energy being drawn from the lake itself following the period of summer-time heat storage. Thus, winter-time maximum evaporation and convective heat losses were concentrated in two- to three-day-long events which were likely initiated by the passage of cold fronts (cool, windy, and dry conditions) and were delayed 5 months after the time of maximum energy inputs. These characteristics can have a large impact on adjacent terrestrial surfaces,

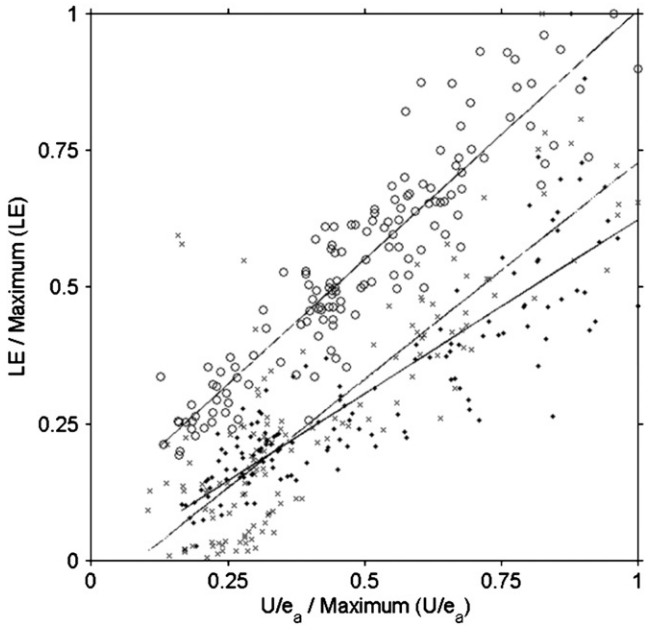

Fig. 10. Scatter plot (points) with linear regressions (lines) showing the relationship between the 0.5-h latent heat flux (λE) and the ratio U/e_a, each divided by the maximum value observed for three example evaporation events shown in Fig. 8. These events occurred during October 9–12, 2009 (solid circles; solid lines), December 14–17, 2009 (open circles; dashed lines), and August 24–27, 2010 (crosses; dotted lines).

for example, through lake-effect snow, fog and cloud formation, and air and wind modifications (e.g. a warmer fall and a cooler spring).

In addition to these unique surface energy balance properties measured on Lake Superior, the presence of ice on the lake abruptly and dramatically alters the surface energy balance. With ice formation in the late fall/winter, the surface albedo increases substantially, and the evaporative water and sensible heat losses decrease due to a steadily decreasing ice-free surface area. Thus, there is an abrupt threshold-like change in the surface energy balance in regions of the lake which transition from ice-free to ice-covered. In the spring, the break-up of ice cover and exposure of open water results in an increase in heat storage and an increase in water temperature with minimal latent or sensible heat losses until the following fall/winter when that stored heat is released. Thus, as shown by Rouse et al. (2003), the timing of the spring ice break-up and fall ice formation dates are as important as the duration (and areal extent) of ice coverage.

Our direct measurements show that the evaporative water loss in water year 2008–2009 (Year 1: 464 mm) was 28% lower than in 2009–2010 (Year 2: 645 mm), and that this loss was proportional to wind speed and inversely proportional to vapor pressure for both years. On the other hand, a higher fraction of the water-year evaporative loss occurred during October–March of 2008–2009 (88%) than for the same 6-month period in 2009–2010 (70%). This indicates that the increase in evaporation rates from Year 1 to Year 2 was associated with changes not only during the cold season, but also during the period April–September (when evaporation rates are typically much smaller). Large difference in ice cover were noted between the two years, with the ice coverage at the end of the October–March evaporation season much less in the high evaporation year (Year 2: 31% maximum ice coverage) compared to the year with the lower evaporation (Year 1: 90% maximum ice coverage). As noted above, the low ice coverage in Year 2 was associated not only with enhanced evaporation rates in late winter (compared to Year 1), but also higher evaporation rates during the subsequent summer and early fall. In addition, it is evident that the high-ice year initially experienced higher evaporation rates in the autumn (Fig. 5), which presumably contributed to the more rapid decline in water temperatures and greater ice coverage that winter. Thus, these observations highlight the complexity of lake ice–evaporation interactions and the need for properly understanding seasonal variability, temporal lags, and ice-evaporation feedbacks.

The dramatic contrast in ice conditions from 2008–2009 to 2009–2010 has been linked to larger-scale atmospheric circulation patterns. For example, during the severe ice conditions that developed during the 2008–2009 winter, Wang et al. (2010) showed a winter teleconnection pattern between the Great Lakes and Arctic regions through the Icelandic low-pressure center. The Icelandic low, in turn, was combined with the strong positive phase of the Arctic Oscillation. Combined with typical La Niña winter conditions (cold surface air temperature), this teleconnection effectively advected cold, dry air over the Great Lakes, thus enhancing evaporation (at least initially), reducing lake surface temperatures, and increasing ice cover. During the winter of 2009–2010, however, a strong El Niño event (warm surface air temperature) resulted in predominately zonal (west-to-east) air transport across the Great Lakes region, fewer frontal storms, and therefore higher-than-normal temperatures and lower ice cover (Bai et al., in press). Thus, it is the combination of both Pacific and Arctic oscillations in sea-level

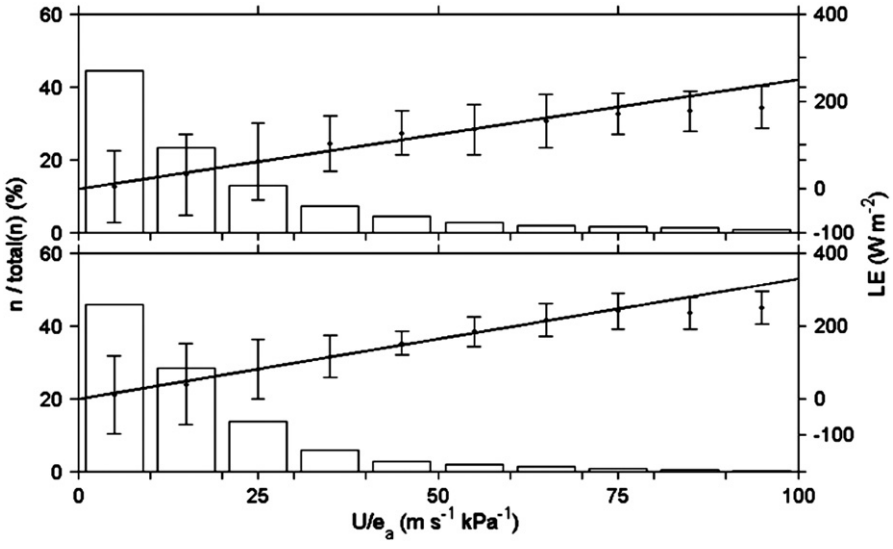

Fig. 11. Relationship between the 0.5-h latent heat flux (λE) and the ratio of the 0.5-h horizontal wind speed to vapor pressure (U/e_a) for the 2008–2009 (top panel) and 2009–2010 (bottom panel) water years. Median values of λE over U/e_a bins of 10 m s^{-1} kPa^{-1} with plus/minus one standard deviation error bars, are shown, along with the percentage of 0–5 h observations in each bin (bars). Cumulatively, 99.1% of the observations were reached by the eighth bin. Lines are robust linear regressions based on the 0.5-h data (not the median binned values), given as $\lambda E = 2.51U/e_a - 1.27$ ($r = 0.55$), and $\lambda E = 3.31U/e_a - 2.25$ ($r = 0.52$), 2008–2009 and 2009–2010, respectively.

pressure, connected over vast distances, that can help explain the large interannual variation in ice cover between the two years.

While the greater ice coverage in Year 1 was most certainly associated with reduced wintertime evaporation (compared to Year 2), as well as lower evaporation in the subsequent summer and fall, the greater ice coverage did not decrease the lake heat content enough to limit the following winter's evaporation rates (in part due to the strong El Niño conditions that developed during 2009–2010). Although net radiation was lower in Year 2 compared to Year 1, air temperatures were higher, thereby reducing the lake/air temperature gradient, and as a result, the sensible heat loss. Thus, the heat capacity of the lake was still adequate to supply energy for winter evaporation in Year 2, and reductions in ice cover and warm spring conditions contributed to higher evaporation rates in the late summer and early fall of 2009–2010. Although our study only includes data from two winter seasons, it is evident that the year with the higher ice coverage had roughly 28% lower water-year evaporation than the low-ice year. While this difference in evaporation rates is not small, it is interesting to note that these back-to-back years had nearly record maximum and minimum ice coverage, yet by the end of the maximum ice cover date (March), the cumulative evaporative water loss difference was only 10% between the two years, indicating the complex control of ice cover on seasonal evaporation and the need to consider more than just the winter ice period.

As shown, the large losses of heat from the lake during the cold season (through both evaporation and sensible heat) are driven by wind events and the large pool of stored heat from within the lake itself, 5 months after net radiation is at its maximum near the summer solstice. This fall and winter heat loss from Lake Superior rapidly lowers the water temperature, and, if below the freezing point, promotes near-shore ice formation. For example, a sustained heat loss of 300 W m^{-2} that we commonly observed during the winter period (e.g., over 3 months) is equivalent to a water temperature decrease of 3.8 °C over the mean depth of 148 m. With climate warming in the Great Lakes region, evaporation and sensible heat loss from the lake have likely increased (Hanrahan et al. 2010; Moitee and McBean, 2009). Over-lake wind speeds have increased in response to larger lake-air temperature gradients (Desai et al., 2009; Rouse, 2009), and this has likely contributed to the higher evaporation rate. Thus, despite a warming climate and higher water temperatures (particularly in summer), negative feedbacks from enhanced evaporative and sensible cooling in the autumn and winter can help to limit the impacts of warming on delayed ice formation, particularly near the shoreline (where ice is likely to form every year, even during mild winters). The same feedbacks can limit climate-induced warming of near-shore temperatures in summertime. It is likely, therefore, that ongoing and future

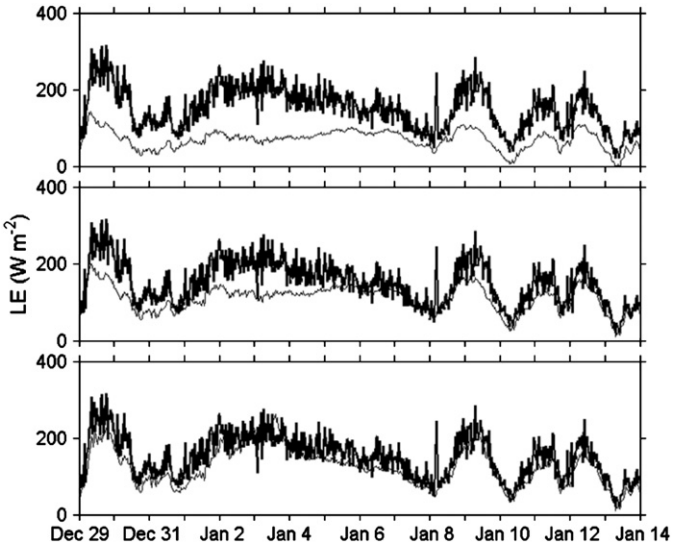

Fig. 12. Measured (thick lines) and modeled (thin lines) 30-min mean latent heat fluxes from December 29, 2009 through January 14, 2010. Modeled λE were based on linear regressions of λE against horizontal wind speed (U; top panel), $\lambda E/U$ against vapor pressure (e_a; middle panel), and λE against U/e_a (bottom panel) using all of the measured data. See Table 3 for summary statistics.

Table 3
Summary statistics based on linear regressions for the measured versus modeled λE shown in Fig. 11. All means were significantly different at a 5% significance level (two-tailed t-test; unequal variance).

Equation	Slope	Intercept (W m^{-2})	r^2	RMSE (W m^{-2})
$\lambda E = 7.08U - 12.75$	0.32	22.3	0.52	17.11
$\lambda E = U(-6.24e_a + 11.26)$	0.48	39.4	0.63	20.43
$\lambda E = 2.87U/e_a + 1.23$	0.77	8.65	0.71	27.28

impacts of climate change will have a somewhat greater impact on offshore conditions in Lake Superior, as opposed to near-shore temperatures and ice cover.

Conclusions

There are multiple indications that warming is occurring in the Great Lakes region; both air and water temperatures are increasing, wind speeds are increasing, and the areal extent of ice cover is decreasing. From our measurements and analysis of the annual surface energy balance of Lake Superior over a 2.5-year period, and supported by our research on other large North American lakes, evaporative and sensible heat loss from the lake under a warming scenario should therefore increase. The majority of the evaporative and sensible heat loss occurred during the autumn and winter, with evaporation directly proportional to the horizontal wind speed, and inversely proportional to the ambient vapor pressure. The five-month delay between maximum summertime energy inputs and wintertime energy outputs indicates that the energy source for the winter season heat loss is the internal energy of the lake itself (and, by inference, the previous summer's radiative inputs). Thermodynamically, evaporative and sensible heat losses act as negative feedbacks to dampen further warming and reductions in ice cover, particularly in near-shore regions.

With both the observational and modeled results that Lake Superior is warming, we anticipate changes in evaporation and ice cover on two time scales. In the short term (e.g., decades), warming will likely result in increased summer evaporation due to higher surface water temperatures and higher wind speeds, while winter evaporation will likely increase in response to decreased mid-lake ice coverage. Near-shore ice duration, however, may be less susceptible to changes due to the more responsive and rapid cooling of shallow water. Over the long term (e.g., centuries) evaporation in the summertime may increase to such an extent that the evaporative seasonal cycle becomes significantly dampened, even in the complete absence of winter ice cover. This would be similar to what is presently observed over southern North American (Liu et al., 2009), as well as tropical fresh water bodies (Verburg and Antenucci, 2010). Better understanding of the processes controlling seasonal heat loss from Lake Superior using direct measurements will help to improve model estimates of lake evaporation, as well as provide more realistic predictions of the potential impacts of climate change.

Acknowledgments

We thank the International Joint Commission — International Upper Great Lakes Study for their generous financial support of this project. The views and opinions presented here, however, are not necessarily those of the International Joint Commission. We thank Wayne Rouse for providing critical input to this work at many stages, including reviewing the final draft. Jia Wang, Anne Clites, and Ray Assel at NOAA-GLERL kindly provided the lake-wide ice-cover data. We also thank the anonymous reviewers, editor, and staff of the Journal of Great Lakes Research for their time and effort that went into improving this manuscript.

References

Argyilan, E.P., Forman, S.L., 2003. Lake level response to seasonal climatic variability in the Lake Michigan–Huron system from 1920 to 1995. J. Great Lakes Res. 29 (3), 488–500.

Assel, R.A., 2005. Great Lakes weekly ice cover statistics. NOAA Technical Memorandum GLERL-113. NOAA Great Lakes Environmental Laboratory, Ann Arbor, MI. 27 pp.

Assel, R.A., Cronk, K., Norton, D., 2003. Recent trends in Laurentian Great Lakes ice cover. Clim. Change 57 (1–2), 185–204.

Austin, J.A., Colman, S.M., 2007. Lake Superior summer water temperatures are increasing more rapidly than regional air temperatures: a positive ice-albedo feedback. Geophys. Res. Lett. 34 (6), L06604.

Bai, X., Wang, J., Colton, M., Liu, Q., Wang, D., Liu, Y., in press. Severe ice conditions in the Bohai Sea, China and mild ice conditions in the Great Lakes during the 2009/2010 winter: links to El Niño and a strong negative Arctic oscillation. J. App. Meteorol. Climatol. (Electronic publication ahead of print). doi:10.1175/2011JAMC2675.1.

Baldocchi, D.D., Hicks, B.B., Meyers, T.P., 1988. Measuring biosphere–atmosphere exchanges of biologically related gases with micrometeorological methods. Ecology 69 (5), 1331–1340.

Beletsky, D., Saylor, J.H., Schwab, D.J., 1999. Mean circulation in the Great Lakes. J. Great Lakes Res. 25 (1), 78–93.

Bennington, V., McKinley, G.A., Kimura, N., Wu, C.H., 2010. General circulation of Lake Superior: mean, variability, and trends from 1979 to 2006. J. Geophys. Res. 115, C12015.

Blanken, P.D., Rouse, W.R., Culf, A.D., Spence, C., Boudreau, L.D., Jasper, J.N., Kochtubajda, B., Schertzer, W.M., Marsh, P., Verseghy, D., 2000. Eddy covariance measurements of evaporation from Great Slave Lake, Northwest Territories, Canada. Water Resour. Res. 36 (4), 1069–1077.

Blanken, P.D., Rouse, W.R., Schertzer, W.M., 2003. Enhancement of evaporation from a large northern lake by the entrainment of warm, dry air. J. Hydrometeorol. 4 (4), 680–693.

Blanken, P.D., Rouse, W.R., Schertzer, W.M., 2008. The time scales of evaporation from Great Slave Lake. In: Woo, M.-K. (Ed.), Atmospheric Dynamics of a Cold Region: The Mackenzie GEWEX Study Experience Volume II. Springer, pp. 181–196.

Businger, J.A., Wyngaard, J.C., Izumi, Y., Bradley, E.F., 1971. Flux-profile relationships in the atmospheric surface layer. J. Atmos. Sci. 28 (2), 181–189.

Cordeira, J.M., Laird, N.F., 2008. The influence of ice cover on two lake-effect snow events over Lake Erie. Mon. Weather. Rev. 136 (7), 2747–2763.

Derecki, J.A., 1981. Operational estimated of Lake-Superior evaporation based on IFGLY findings. Water Resour. Res. 17 (5), 1453–1462.

Desai, A.R., Austin, J.A., Bennington, V., McKinley, G.A., 2009. Stronger winds over a large lake in response to weakening air-to-lake temperature gradient. Nat. Geosci. 2, 855–858.

Ellis, A.W., Johnson, J.J., 2004. Hydroclimatic analysis of snowfall trends associated with the North American Great Lakes. J. Hydrometeorol. 5, 471–486.

Hanrahan, J.L., Kravtsov, S.V., Roebber, P.J., 2010. Connecting past and present climate variability to the water levels of Lakes Michigan and Huron. Geophys. Res. Lett. 37, L01701.

Hartmann, H., 1990. Climate change impacts on Laurentian Great Lakes levels. Clim. Change 17 (1), 49–67.

Horst, T.W., 1997. A simple formula for attenuation of eddy fluxes measured with first-order-response scalar sensors. Boundary Layer Meteorol. 8 (2), 219–233.

Huang, A., Rao, Y.R., Lu, Y., Zhao, J., 2011. Hydrodynamic modeling of Lake Ontario: an intercomparison of three models. J. Geophys. Res. 115, C12076.

Kalff, J., 2002. Limnology. Prentice Hall, New Jersey.

Kunkel, K.E., Palecki, M.A., Hubbard, K.G., Robinson, D.A., Redmond, K.T., Easterling, D.R., 2007. Trend identification in twentieth-century US snowfall: the challenges. J. Atmos. Oceanic Technol. 24 (1), 64–73.

Laird, N.F., Kristovich, D.A.R., 2002. Variations of sensible and latent heat fluxes from a Great Lakes buoy and associated synoptic weather patterns. J. Hydrometeorol. 3 (1), 3–12.

Lenters, J.D., 2001. Long-term trends in the seasonal cycle of Great Lakes water levels. J. Great Lakes Res. 27 (3), 342–353.

Lenters, J.D., 2004. Trends in the Lake Superior water budget since 1948: a weakening seasonal cycle. J. Great Lakes Res. 30 (Supplement 1), 20–40.

Liu, H., Zhang, Y., Liu, S., Jiang, H., Sheng, L., Williams, Q.L., 2009. Eddy covariance measurements of surface energy budget and evaporation in a cool season over southern open water in Mississippi. J. Geophys. Res. 114, D04110.

Liu, H., Blanken, P.D., Weidinger, T., Nordbo, A., Vesala, T., 2011. Variability in cold front activities modulating cool-season evaporation from a southern inland water in the USA. Environ. Res. Lett. 6, 024022.

Lofgren, B.M., Zhu, Y.C., 2000. Surface energy fluxes on the Great Lakes based on satellite-observed surface temperatures 1992 to 1995. J. Great Lakes Res. 26 (3), 305–314.

Massman, W.J., 2000. A simple method for estimating frequency response corrections for eddy covariance systems. Agric. For. Meteorol. 104 (3), 185–198.

Moitee, H., McBean, E., 2009. An assessment of long-term trends in hydrologic components and implications for water levels in Lake Superior. Hydrol. Res. 40 (6), 564–579.

Nghiem, S.V., Leshkevich, G.A., 2007. Satellite SAR remote sensing of Great Lakes ice cover, Part 1: ice backscatter signatures at C band. J. Great Lakes Res. 33 (4), 722–735.

Nordbo, A., Launianen, S., Mammarella, I., Leppäranta, M., Huotari, A., Ojala, A., Vesala, T., 2011. Long-term energy flux measurements and energy balance over a small boreal lake using eddy covariance technique. J. Geophys. Res. 116, D02119.

Quinn, F.H., 2002. Secular changes in Great Lakes water level seasonal cycles. J. Great Lakes Res. 28 (3), 451–465.

Rouse, W.R., 2009. Atmospheric science: high winds over Lake Superior. Nat. Geosci. 2 (12), 827–828.

Rouse, W.R., Oswald, C.M., Binyamin, J., Blanken, P.D., Schertzer, W.M., Spence, C., 2003. Interannual and seasonal variability of the surface energy balance and temperature of central Great Slave Lake. J. Hydrometeorol. 4 (4), 720–730.

Schertzer, W.M., 1978. Energy budget and monthly evaporation estimates for Lake Superior, 1973. J. Great Lakes Res. 4 (3–4), 320–330.

Schertzer, W.M., Rao, Y.R., 2009. An overview of the characteristics of Lake Superior meteorology, hydrology and physical limnology. In: Munawar, M., Munawar, I.F. (Eds.), State of Lake Superior, Ecovision World Monograph Series.

Schuepp, P.H., LeClerc, M.Y., MacPherson, J.I., Desjardines, R.L., 1990. Footprint prediction of scalar fluxes from analytical solutions of the diffusion equation. Boundary Layer Meteorol. 50 (1–4), 353–373.

Sellinger, C.E., Stow, C.A., Lamon, E.C., Qian, S.S., 2008. Recent water level declines in the Lake Michigan–Huron system. Environ. Sci. Technol. 42 (2), 367–373.
Spence, C., Blanken, P.D., Hedstrom, H., Fortin V., Wilson H., in press. Evaporation from Lake Superior 2: spatial extent and variability. J. Great Lakes Res.
Tanny, J., Cohen, S., Assouline, S., Lange, F., Grava, A., Berger, D., Teltch, B., Parlange, M. B., 2007. Evaporation from a small water reservoir: direct measurements and estimates. J. Hydrol. 351, 218–229.
United States Army Corps of Engineers, 2008. Great Lakes Recreational Boating. Washington, DC, 93 pp.
Verburg, P., Antenucci, J.P., 2010. Persistent unstable atmospheric boundary layer enhances sensible and latent heat loss in a tropical great lake: Lake Tanganyika. J. Geophys. Res. 115, D11109.
Wang, J., Bai, X., Leshkevich, G.A., Colton, M.C., Clites, A.H., Lofgren, B.B., 2010. Severe ice cover on Great Lakes during winter 2008–2009. EOS Trans. 91 (5), 41–42.
Webb, E.K., Pearman, G.I., Leuning, R., 1980. Correction of flux measurements for density effects due to heat and water-vapor transfer. Q. J. R. Meteorolog. Soc. 106 (447), 85–100.